Supporting information

Confinement and passivation of perovskite quantum dots in porous natural palygorskite toward efficient and ultrastable light-harvesting system in water

Genping Meng,[a‡] Xijiao Mu,[a‡] Liping Zhen,[a] Jun Hai,[a] Zefan Zhang,[a] Tianzhi Hao,[a] Siyu Lu*[c], Aiqin Wang*[b], and Baodui Wang*[a]

‡*These authors contributed equally to this work.*

Corresponding author: Siyu Lu, sylu2013@zzu.edu.cn; Aiqin Wang, aqwang@licp.cas.cn; Baodui Wang, wangbd@lzu.edu.cn.

Table of Contents

S1. Materials and Instrumentation

Materials:

All reagents and deuterated chloroform were commercially available unless otherwise stated. The reagents and solvents were dried according to the standard procedures described in literature. Palygorskite (ATP) was supplied by Aiqin Wang, a professor at Lanzhou Institute of Chemical Physics, Chinese Academy of Sciences. Cs-Oleate was prepared according to the published procedure. Caesium carbonate (Cs_2CO_3, 99.9%) was abtained from Aladdin Reagent. Lead chloride ($PbCl_2$, 100.0%), Lead bromide ($PbBr_2$, 99.0%), Lead iodide (PbI_2, 99.99%) were purchased from ITC, Octadecene (ODE, 90%), oleic acid (OA, 90%) and Oleylamine (70 %) were obtained from Sigma. *N,N*-dimethylaniline (99%), indole (99%), 5-bromoindole (98%), 5-methylindole (98%), rose bengal (BR) and eosin Y(BR) were purchased from MACKLIN Reagent. The abbreviation for solvent was listed here: *N,N*-dimethylformamide (DMF), Toluene (PhMe).

Instrumental techniques: Transmission electron microscopy (TEM) and high-resolution TEM investigations were carried out on a FEI Talos 200s electron microscope operating at an accelerating voltage of 200 kV. Samples for TEM analysis were prepared by dropping a dilute solution of composites onto ultrathin carbon-coated copper grids. Morphology of samples were performed by Field emission Scanning Electron Microscope (SEM, FEI, Sirion 200) with an accelerating voltage of 15 kV. Powdered X-ray diffraction (PXRD) patterns were recorded on AXS D8-Advanced diffractometer with Cu Ka radiation. The nitrogen adsorption-desorption isotherms were acquired through a high precision Autosorb apparatus at 77.35 K, and Non-Local Density Functional Theory (NLDFT) method was applied to the adsorption branch to calculate the pore size distribution of samples. X-ray photoelectron spectroscopy (XPS, a PHI-5702 multifunctional spectrometer) measurements were investigated using Al Kα radiation. Fourier transform infrared (FTIR) spectra were performed on a Nicolet FT-170SX spectrometer at room temperature. Ultraviolet and visible absorption (UV-vis) measurements were recorded on Shimadzu UV-1750 at room temperature. UV/Vis diffuse reflectance spectroscopy (DRS) were measured on a UV-2006 UV-Specterophotometer. Photocatalysis was performed using Xenon lamp (HSXF/UV 300), equipped with 400-800 nm filter. Photoluminescence (PL) spectra were acquired on an Edinburgh Instruments FLS920 fluorescence spectrometer. ^{1}H-NMR spectra were recorded in $CDCl_3$ on a JEOL ESC 400 MHz instrument. Chemical shifts for ^{1}H-NMR spectra are reported in parts

per million (ppm, δ scale) downfield from tetramethylsilane, and referenced internally to the residual proton in the solvent ($CDCl_3$: δ 7.26). Data are reported as follows: Chemical shift, multiplicity (s = singlet, d = doublet, t = triplet, q = quartet, m = multiplet), coupling constants. *J*, are reported in hertz. The absolute quantum yields were measured on a horiba fl-3 instrument with the integrating sphere. Time-resolved PL decay curves were measured on a horiba fl-3 instrument and fitted to a biexponential (see **eqs S1** and **S2**) decay curves of

$$A(t) = A_1 \exp\left(-\frac{t}{\tau_1}\right) + A_2 \exp\left(-\frac{t}{\tau_2}\right) \qquad \textbf{eq S1}$$

The average lifetimes were calculated using

$$\tau_{avg} = (A_1{\tau_1}^2 + A_2{\tau_2}^2)/(A_1\tau_1 + A_2\tau_2) \qquad \textbf{eq S2}$$

S2. Experimental procedure and methods

Synthesis of Cs-Oleate.

Cs-Oleate (CsOA) was synthesized according to the previous literature and slightly modified.[1] Oleic acid (2.5 mL), octadecene (10 mL, ODE) and oleylamine (0.1 mL) were syringed into a 100 mL 3-neck flask containing 0.814 g of Cs_2CO_3 (2.50 mmol). The resulting mixture was dried at 120 °C for 1 h and then reacted at 150 °C under N_2 atmosphere for 2h. Since CsOA will precipitate out of ODE at room temperature, it has to be preheated to dissolve before usage.

Preparation of $CsPbBr_3$ QDs without PAL matrix.

In a typical preparation of $CsPbBr_3$ quantum dots (QDs) without PAL matrix. DMF (1 mL) and $PbBr_2$ (0.05 mmol) were loaded into a 5 mL flask. After complete solubilization of $PbBr_2$, Cs-oleate solution (0.05 mL, 0.4 mol/L in ODE, prepared as shown in above) was added. Finally, 0.05 mL of mixed solution was added into a new flask along with dried PhMe (2 mL).

Photostability and thermostability of $CsPbBr_3$@PAL antenna

To evaluate the photostability of the prepared $CsPbBr_3$@PAL antenna, the $CsPbBr_3$@PAL powder was packed into vial and illuminated with 365 nm LED lamp (10 W) at room temperature. To analyze the thermostability of the synthesized $CsPbBr_3$@PAL antenna, the $CsPbBr_3$@PAL powder was packed into glass plates with a groove, which was then heated at 150 °C. During the heating-cooling cycle at 30-150°C, photoluminescence (PL) spectra were collected at an interval of 20 °C.

Energy transfer efficiency ($\boldsymbol{\Phi_{ET}}$) calculation[2]

The energy-transfer efficiency ($\boldsymbol{\Phi_{ET}}$) was calculated using equation **S3**:

$\boldsymbol{\Phi_{ET} = 1 - I_{DA}}$, ($\lambda_{ex}$ = donor)/$\boldsymbol{I_D}$, (λ_{ex} = donor) **(eq. S3)**

For ESY-$CsPbBr_3$@PAL, where $\mathbf{I_{DA}}$ and $\mathbf{I_D}$ are the fluorescence intensities of ESY-$CsPbBr_3$@PAL (donor and acceptor) and $CsPbBr_3$@PAL composite (donor) at 516 nm when excited at 365 nm, respectively. The energy-transfer efficiency ($\boldsymbol{\Phi_{ET}}$) was calculated as 72.2% in water, measured under the condition of [$CsPbBr_3$@PAL] = 0.1 mg mL^{-1}, [ESY] = 7.0×10^{-3} mg mL^{-1}, and λ_{ex} = 365 nm.

For RB-$CsPbBr_2I$@PAL system, where $\boldsymbol{I_{DA}}$ and $\boldsymbol{I_D}$ are the fluorescence intensities of RB-$CsPbBr_3$@PAL (donor and acceptor) and ESY-$CsPbBr_3$@PAL (donor) at 539 nm when excited at 365 nm, respectively. The energy-transfer efficiency ($\boldsymbol{\Phi_{ET}}$) was calculated as 65.3% in water, measured under the condition of [$CsPbBr_3$@PAL] = 0.1 mg mL^{-1}, [ESY] = 7.0×10^{-3} mg mL^{-1}, [RB] = 9.0×10^{-3}

mg mL^{-1} and λ_{ex} = 365 nm.

Computational Details

In this work, we use first-principles molecular dynamics methods with CP2K/Quickstep[3]to study the collision, adsorption and molecular transfer processes of between water and $CsPbBr_3$@PAL. Molecular dynamics algorithm combined with NVT ensemble, Nose-Hover thermostat[4, 5], 1 fs step size, 500,000 steps. The force and velocity are calculated using density functional theory (DFT)[6] for BLYP functional[7], Gaussian-type basis set[8] and Goedecker-Teter-Hutter (GTH) pseudopotentials[9,10] combined with Gamma k-point and 400 eV cut-off energy. In the calculation steps, the energy minimization is used to balance the system, and then the Maxwell distribution method is used to give the molecules different collision probabilities, and then the dynamic process is carried out. We analyzed the interaction of molecules and substrates using the independent gradient model (IGM)[11] performed by the Multiwfn-3.6 software[12] using the calculated wave function files.

Photocatalytic reaction in aqueous medium

Figure S1. Structural formulas of ESY and RB.

In a 10 mL pyrex glass tube, 1 mg RB-ESY-$CsPbBr_3$@PAL was suspended in 5 mL of H_2O-MeCN (1:1, v/v) in the presence of indole (0.2 mmol) and *N,N*-dimethylaniline (1.0 mmol, 5 equiv). The reaction mixture was stirred and irradiated by Xenon lamp providing visible light (λ > 420 nm) by using a 420 nm cut-off filter. After that, the resulting mixture was centrifuged and washed. The solution was evaporated under reduced pressure, and the obtained crude compound was purified by column chromatography with petroleum ether/ethyl acetate (20:1) as eluent on silica gel to afford **1c** powder.

S3. Crystal structure of PAL matrix

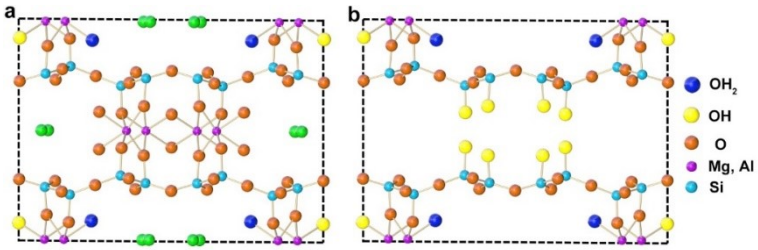

Figure S2. (**a**) Crystal structure of Natural PAL; (**b**) Crystal structure of PAL matrix.

S4. TEM images

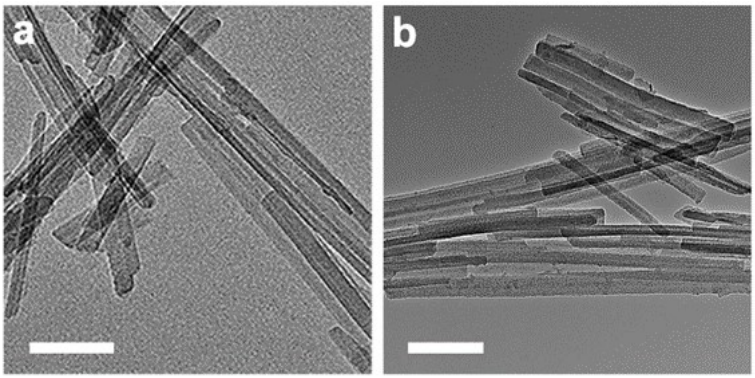

Figure S3. (**a**) TEM image of original PAL nanorods. (**b**) TEM image of PAL matrix. Scale bars: a and b, 100 nm.

The transmission electron microscopy (TEM) images evidence that the palygorskite are maintained fibrous morphology without undergoing damage.

S5. PXRD Patterns

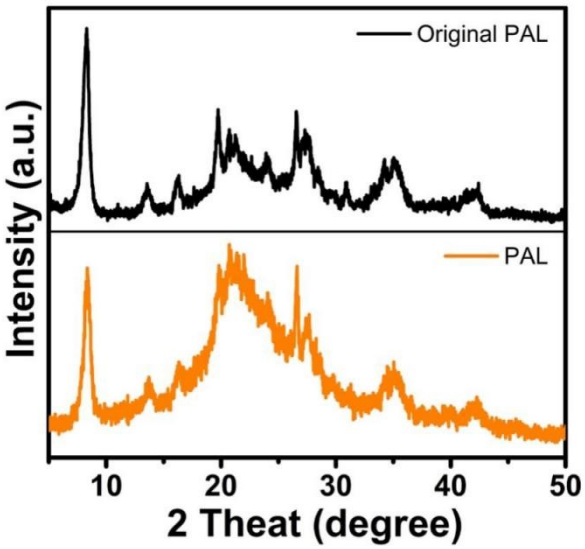

Figure S4. PXRD patterns of original PAL and PAL matrix.

The experimental powder X-ray diffraction (PXRD) patterns evidence that the palygorskite are maintained strong (110) crystal plane during treating process, without undergoing damage.

S6 Pore size distributions of PAL Matrix

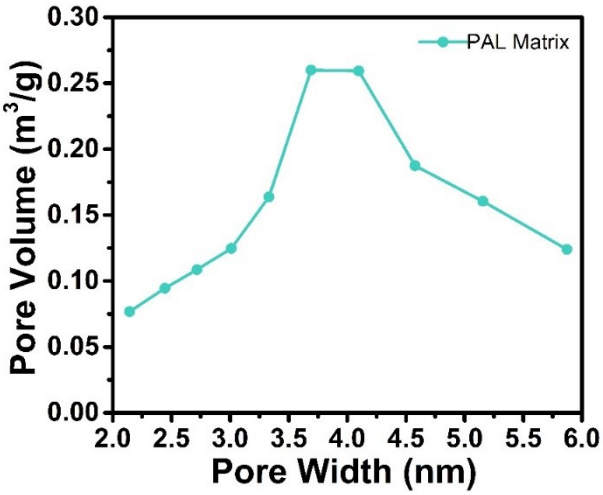

Figure S5. Pore size distributions of PAL Matrix calculation based upon NLDFT.

S7. EDS Mapping of PAL matrix and $PbBr_2$@PAL

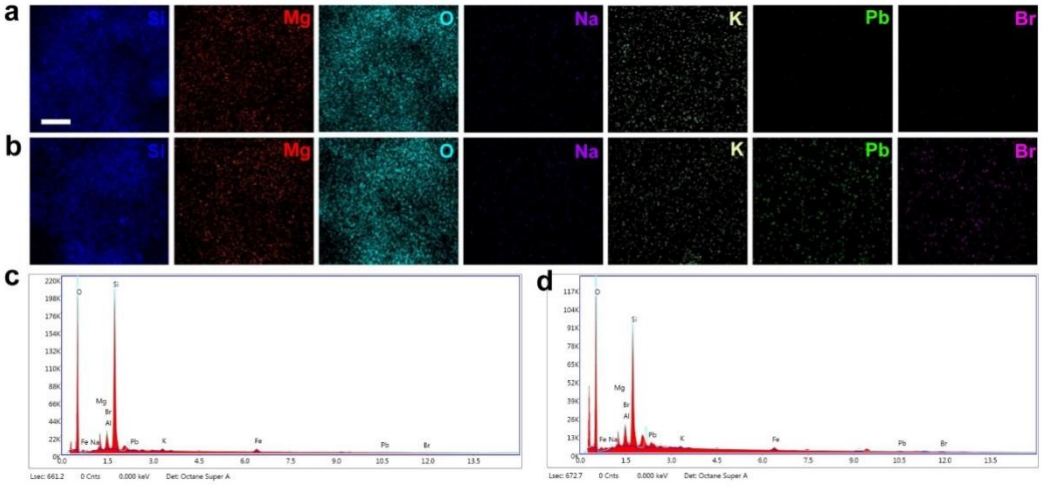

Figure S6. (**a**, **b**) EDS mappings for PAL matrix and $PbBr_2$@PAL, respectively. Scale bars: 5 μm. (**c**, **d**) EDS spectra of PAL matrix and $PbBr_2$@PAL with the elemental composition analysis, respectively.

Table S1. EDS elemental composition analyses of PAL matrix and $CsPbBr_3$@PAL.

Sample	Si (%)	O (%)	Mg (%)	Na (%)	K (%)	Pb	Br
PAL	27.56	65.37	4.60	0.35	0.51	0	0
$PbBr_2$@PAL	25.34	65.72	2.95	0.01	0.33	1.23	1.00

The elemental composition analyses show that content of Mg^{2+}, Na^+ and K^+ decreased after ion exchange, which further confirmed the occurrence of this process.

S8. Size Distribution of as-prepared $CsPbBr_3$ NCs in $CsPbBr_3$@PALcomposite

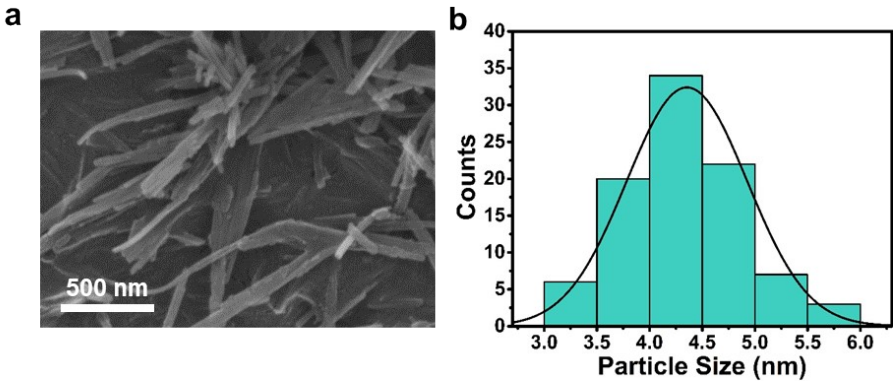

Figure S7. a) The SEM image of the $CsPbBr_3$@PAL antenna. b) Diameter distribution histograms of as-prepared $CsPbBr_3$ NCs in the $CsPbBr_3$@PAL.

The size of $CsPbBr_3$ NCs in the $CsPbBr_3$@PAL composite was estimated by Nano Measurer software and found to almost be in the range of 3.0-6.0 nm.

S9. Pore size distributions of PAL Matrix and CsPbBr3@PALcomposite

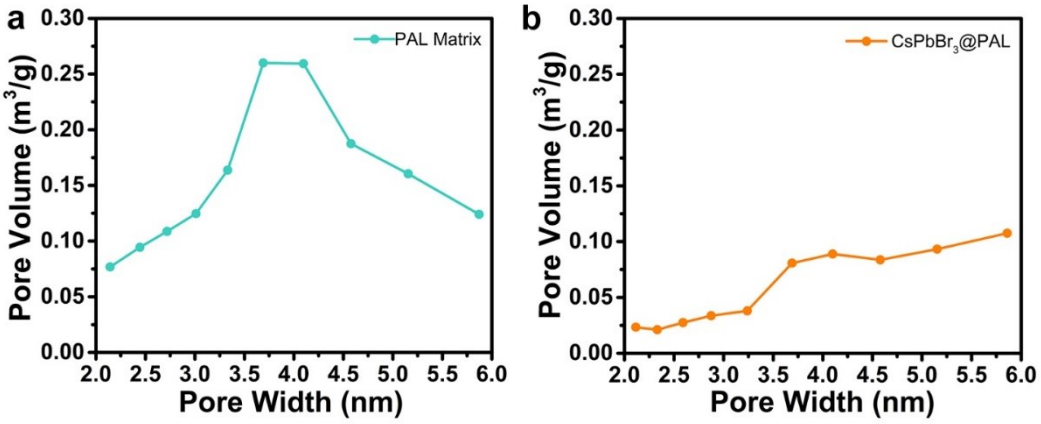

Figure S8. Pore size distributions of PAL Matrix (**a**) and $CsPbBr_3$@PALcomposite (**b**) calculation based upon NLDFT.

It can be see from Figure S6a that the pore size distribution of the matrix is concentrated in 3.0-6.0 nm. The mesoporous pores of PAL matrix matches well with the size of $CsPbBr_3$ QDs, preliminarily suggesting that the growth of perovskite QDs can be well encapsulated by the cavities of natural PAL matrix. The pore volume is decreased after the encapsulation of $CsPbBr_3$ QDs, demonstrating the in-situ growth of $CsPbBr_3$ QDs into the internal pores of PAL matrix.

S10. Elemental EDS Mappings of $CsPbBr_3$@PAL composite

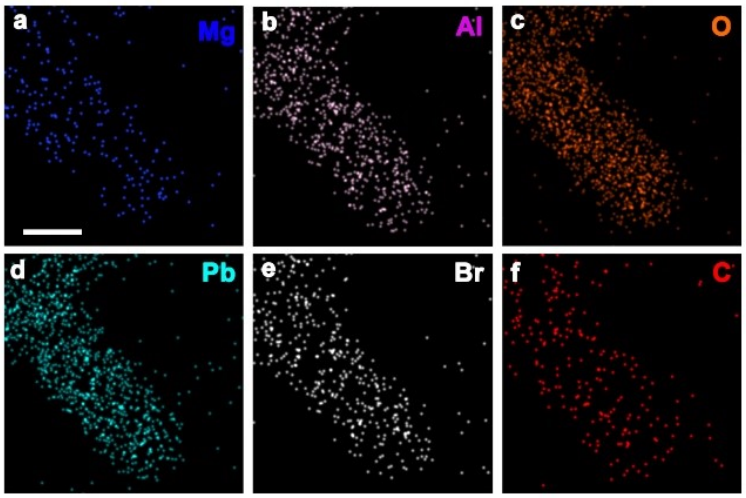

Figure S9. Elemental mapping by EDX for $CsPbBr_3$@PAL composite in **Figure 2.** Scale bars: 30 nm.

S11. IR Spectra

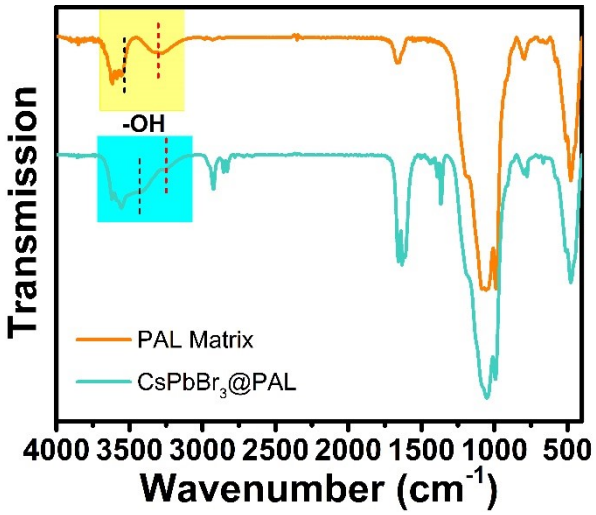

Figure S10. IR spectra of PAL and $CsPbBr_3$@PAL composite.

The characterization of Fourier Transform Infrared (FTIR) spectra reveals that there are H-bonding between the bromide anion of the $CsPbBr_3$ QDs and the functional groups on PAL matrix, which is attributed to -OH vibrational peak of the $CsPbBr_3$@PAL antenna shows a slight shift to lower wavenumber and broadening compared to PAL matrix.

S12. X-ray Photoelectron Spectroscopy (XPS) Study

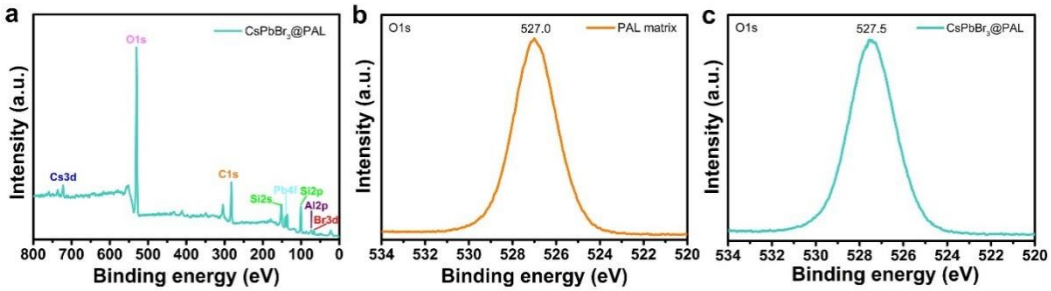

Figure S11. (**a**) XPS spectrum of $CsPbBr_3$@PAL composite; (**b**) O1s spectrum of PAL matrix; (**c**) O1s spectrum of $CsPbBr_3$@PAL composite.

The X-ray photoelectron spectra (XPS) exhibit the characteristic peaks of Cs, Pb, Br, C, Si, Al and O, which are consistent with the elements in $CsPbBr_3$@PAL antenna (Figure S6a). The binding energy related to the oxygen signal shifts from 527.0 eV for PAL matrix to 527.5 eV for the $CsPbBr_3$@PAL antenna (Fig. S5b and c). This phenomenon implies the formation of O-Pb coordination bonds owing to the decrease in the electron density of O atoms.

S13. Digital photos of materials under visible and ultraviolet irradiation

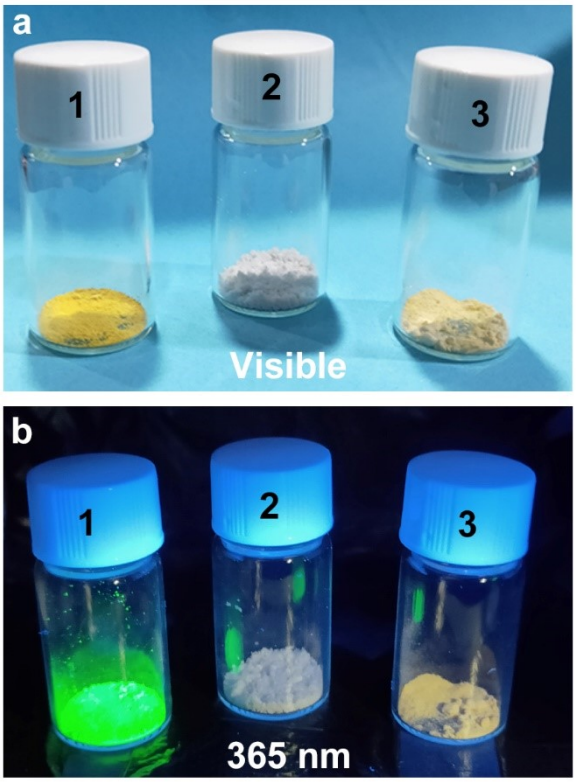

Figure S12. Digital photos of $CsPbBr_3$@PALcomposite under visible (**a**) and ultraviolet irradiation (**b**). Sample **1** is $CsPbBr_3$@PAL antenna; Sample **2** is PAL; Sample **3** is $CsPbBr_3$ QDs.
Sample **1** emits bright green luminescence under ultraviolet irradiation, while sample **3** emits a faintly negligible green fluorescence like sample **2**.

S14 TEM image of $CsPbBr_3$ QDs

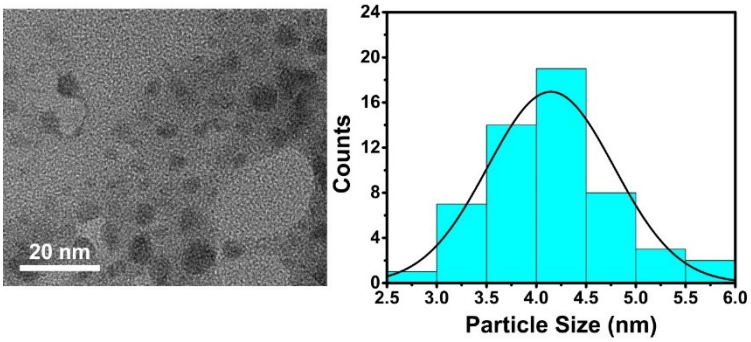

Figure S13. Diameter distribution histograms of $CsPbBr_3$ QDs without PAL matrix.

The size of $CsPbBr_3$ QDs alone were estimated by Nano Measurer software and found to almost be in the range of 2.5-6.0 nm, which is similar to the size of $CsPbBr_3$ QDs in PAL matrix.

S15 Tauc-plot curve

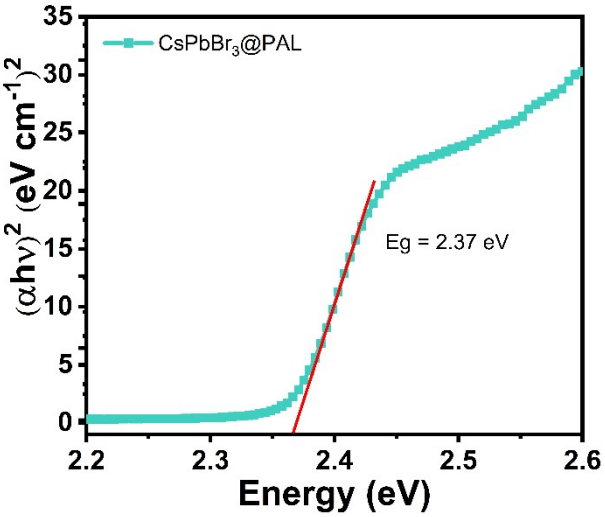

Figure S14. The corresponding Tauc-plot curve of the $CsPbBr_3$@PAL antenna.

S16. Diameter distribution and optical properties of the $CsPbBr_3$ BCs

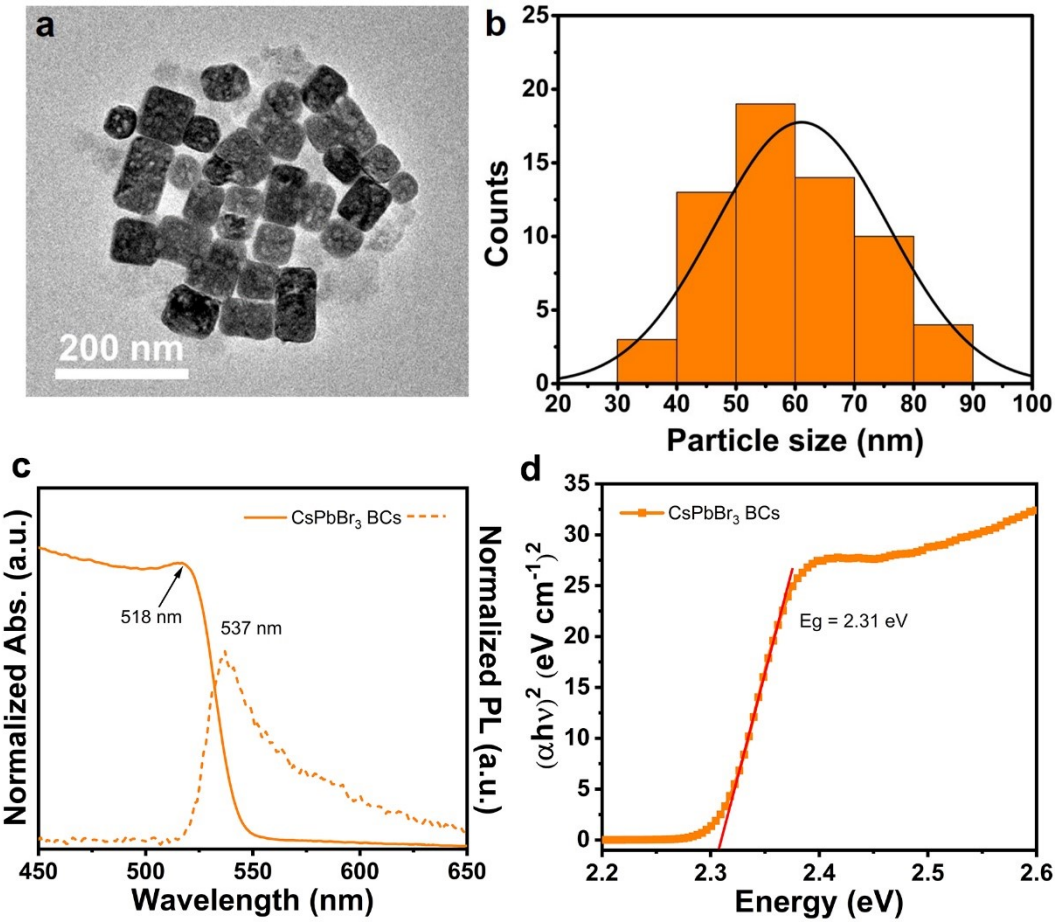

Figure S15. a)TEM image of $CsPbBr_3$ BCs. b) Diameter distribution histograms of $CsPbBr_3$ BCs. c) UV/Vis DRS (solid lines) and PL (dotted lines) spectra of $CsPbBr_3$ BCs. d) The corresponding Tauc-plot curves of the $CsPbBr_3$ BCs.

TEM image shows that the size of CsPbBr3 BCs particles is not uniform, and the particles have holes. The size of CsPbBr3 BCs was estimated by Nano Measurer software and found to almost be in the range of 30-90 nm.

S17. Absolute quantum yield measurement

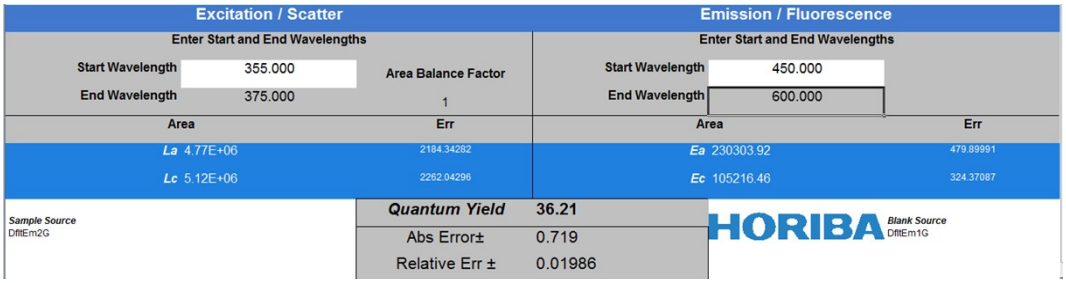

Figure S16. Absolute fluorescence quantum yields of $CsPbBr_3$@PAL antenna in water.

S18. Emission spectra of $CsPbBr_3$ QDs

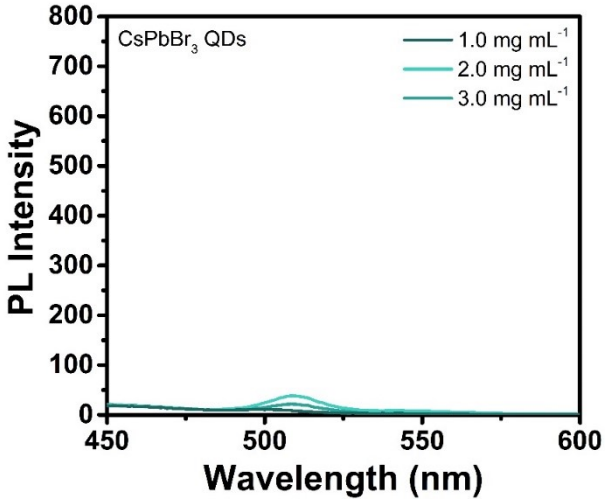

Figure S17. Emission spectra of $CsPbBr_3$ QDs alone in water.

The emission spectra show that the $CsPbBr_3$ QDs alone are extremely unstable in water, showing negligible fluorescence emission even at concentrations as high as 3.0 mg ml^{-1}. Therefore, quantum dots alone cannot construct an artificial light-harvesting system in water, which is also the scientific question addressed by this work.

S19. Immersed in water measurements

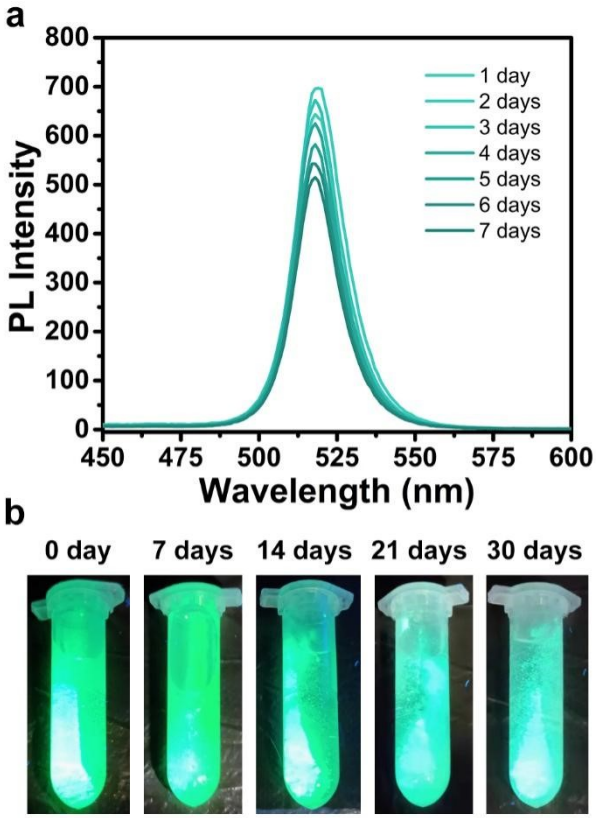

Figure S18. (**a**) PL spectrum of $CsPbBr_3$@PAL antenna immersed in water for 1 week. (**b**) Digital photos of $CsPbBr_3$@PAL antenna immersed in water for 30 days under UV illumination at 365 nm.

S20. Thermal stability measurements

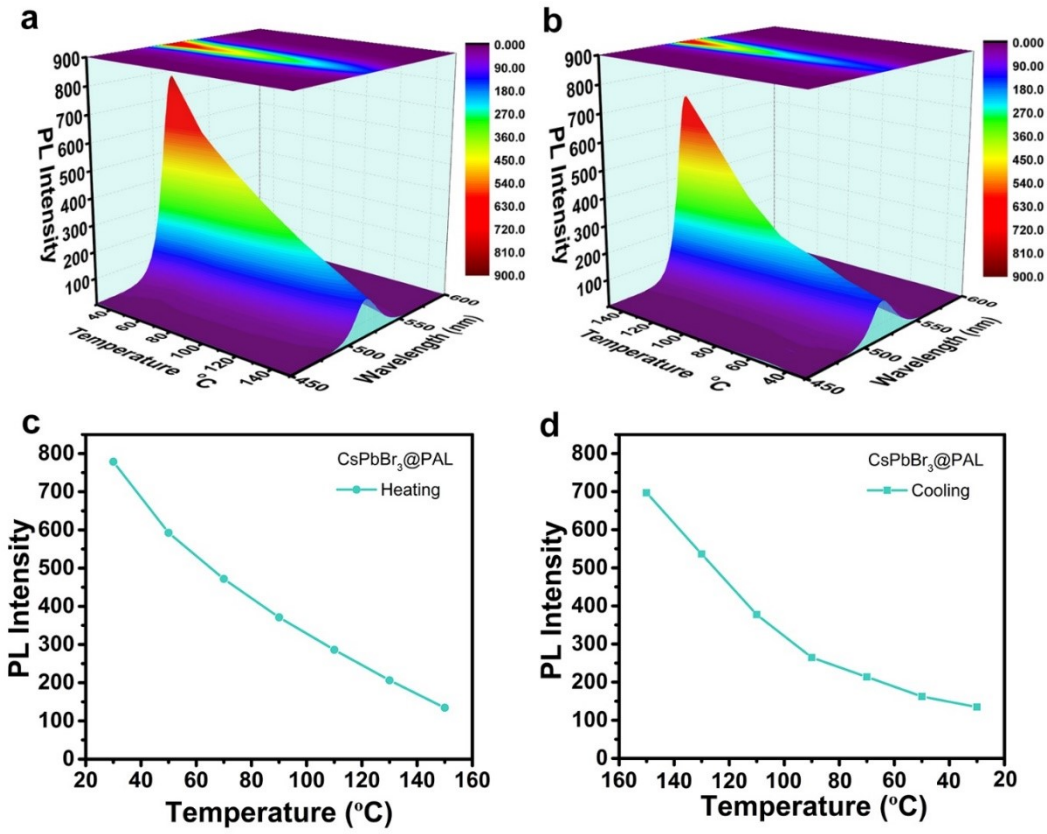

Figure S19. 3D Color Map Surface images (**a**, **b**) and line charts (**c**, **d**) of the temperature-dependent PL for $CsPbBr_3$@PAL antenna, including two processes of heating up and cooling down.

S21. Composition-tunable PL spectra of $CsPbX_3$@PAL composite.

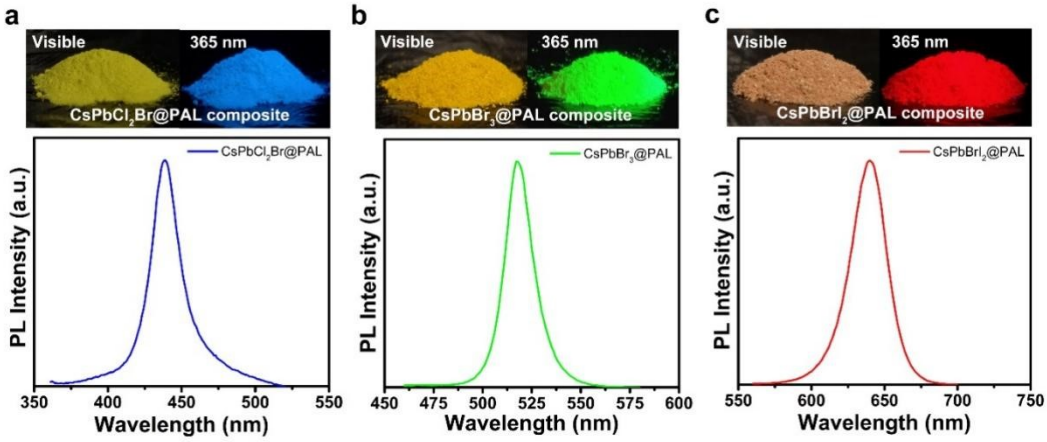

Figure S20. (**a**) Digital photos and PL spectrum of $CsPbCl_2Br$@PAL composite under Visible light and UV illumination at 365 nm. (**b**) Digital photos and PL spectrum of $CsPbBr_3$@PAL composite under Visible light and UV illumination at 365 nm. (**c**) Digital photos and PL spectrum of $CsPbBr_2I$@PAL composite under Visible light and UV illumination at 365 nm.

S22. Degree of spectral overlap

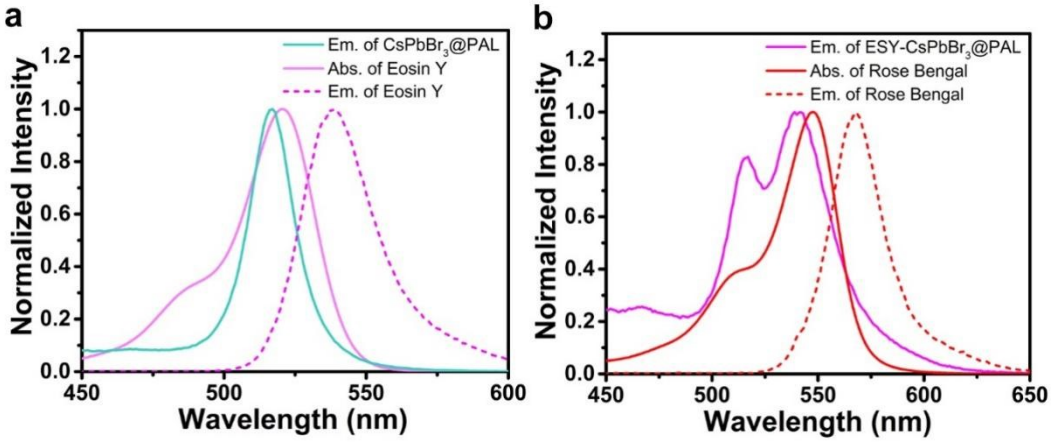

Figure S21. (**a**) Normalized absorption spectrum and emission spectrum of ESY and emission spectrum of $CsPbBr_3$@PAL antenna. (**b**) Normalized absorption spectrum and emission spectrum of ESY-$CsPbBr_3$@PAL assembly and emission spectrum of ESY.

S23. Fluorescence spectra of ALHS and dyes

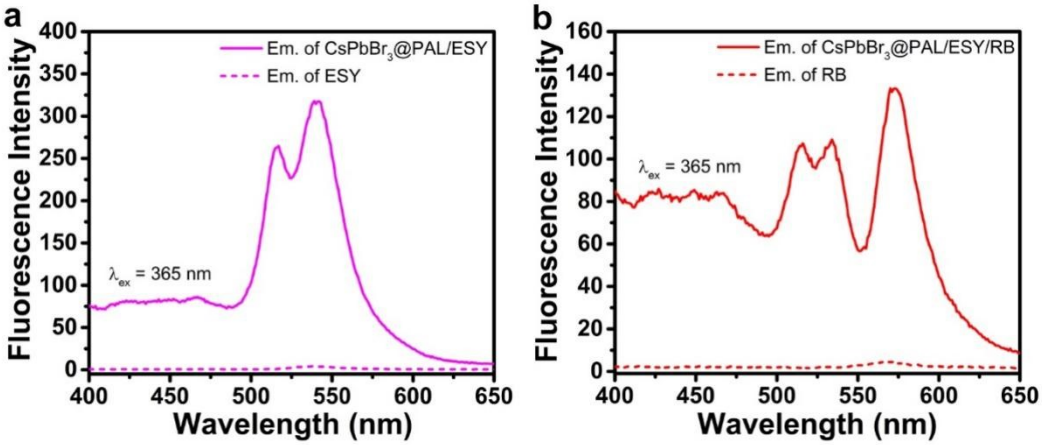

Figure S22. (**a**) Fluorescence spectra of ESY-$CsPbBr_3$@PAL assembly and ESY (λ_{ex} = 365 nm). (**b**) Fluorescence spectra of RB-ESY-$CsPbBr_3$@PAL system and RB (λ_{ex} = 365 nm).

S24. The TRFDS spectra of ESY and RB

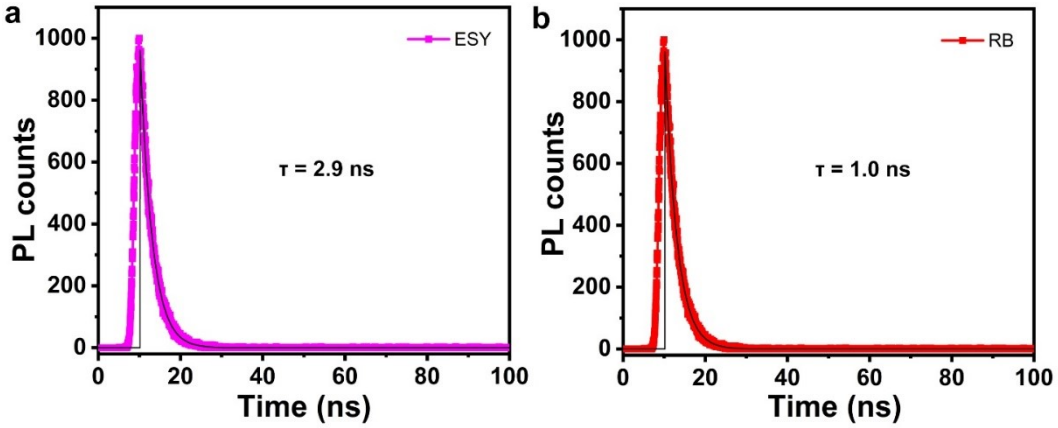

Figure S23. The TRFDS spectra of ESY recorded at λ = 541 nm (**a**) and RB recorded at λ = 570 nm (**b**) in water.

S25. Energy-transfer efficiency calculations

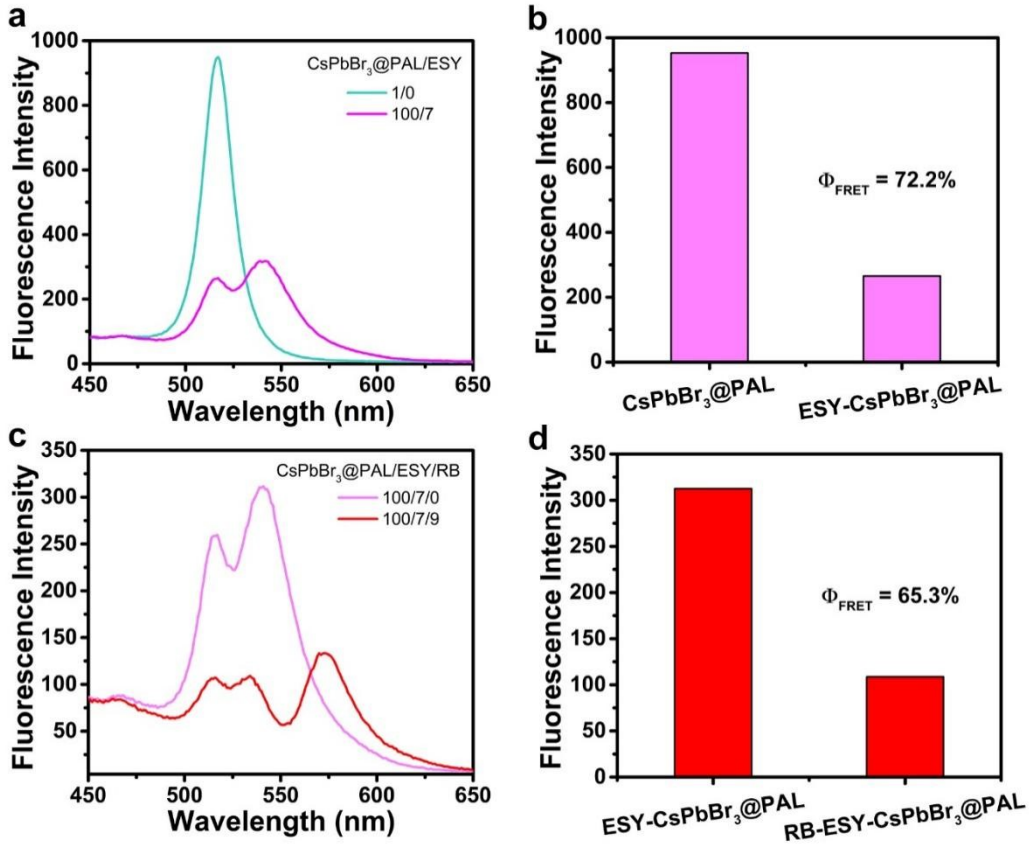

Figure S24. (**a**) Fluorescence spectra of $CsPbBr_3$@PAL composite and ESY-$CsPbBr_3$@PAL. (**b**) The histogram of $CsPbBr_3$@PAL and ESY-$CsPbBr_3$@ PAL emission intensities. (**c**) Fluorescence spectra of ESY-$CsPbBr_3$@PAL and RB-ESY-$CsPbBr_3$@PAL system. (**d**) The histogram of ESY-$CsPbBr_3$@PAL and RB-ESY-$CsPbBr_3$@PAL system emission intensities.

S26. Photographs of $CsPbBr_3$@PAL antenna dispersed in water under visible and ultraviolet irradiation

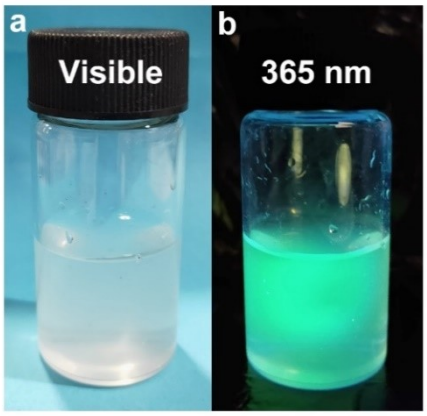

Figure S25. Dispersion in solution of $CsPbBr_3$@PAL antenna.
The $CsPbBr_3$@PAL antenna remained stable dispersion at least 24 h at room temperature, indicating that the hydrophily of PAL matrix can prevent their agglomeration and promote their stability in water.

S27. Emission spectra of $CsPbBr_3$ QDs

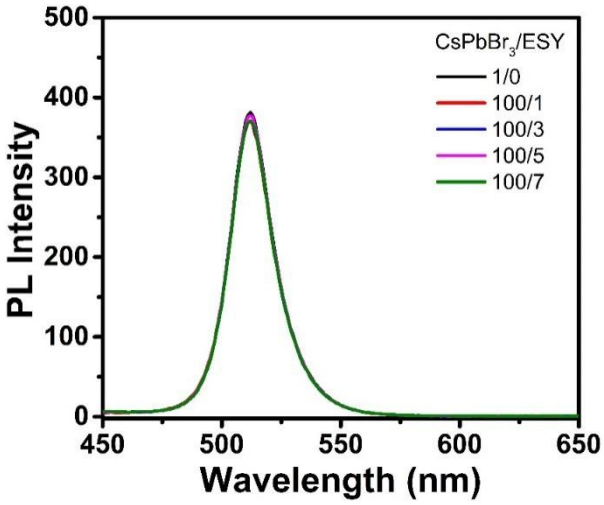

Figure S26. Emission spectra of $CsPbBr_3$ QDs alone with different amounts of ESY.

From the emission spectra, it can be seen that there is almost no energy transfer between the $CsPbBr_3$ QDs alone and the dye, which may be because the distance between the $CsPbBr_3$ QDs alone and the ESY does not meet the requirements of FRET.

S28. Photocatalytic Friedel-Crafts alkylation in aqueous solution

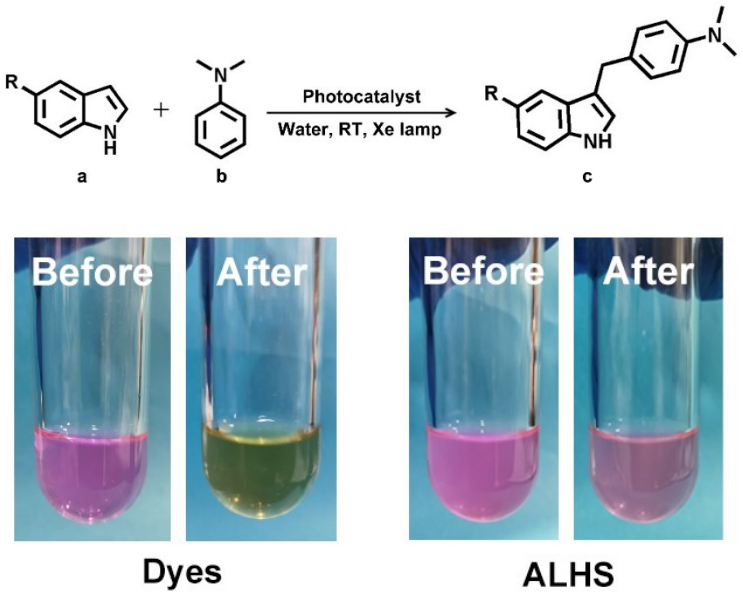

Figure S27. The Photocatalytic Friedel-Crafts alkylation reactivities of indoles with different electronegativity and *N,N*-dimethylaniline to afford 3-arylmethyl indole derivatives in aqueous solution. **2a** is 5-methylindole. **2b** is 5-bromoindole.

In a 10 mL pyrex glass tube, RB-ESY-$CsPbBr_3$@PAL was suspended in 5 mL of H_2O-MeCN (1:1, v/v) in the presence of indoles (0.2 mmol) and *N,N*-dimethylaniline (1.0 mmol, 5 equiv). The reaction mixture was stirred and irradiated by Xenon lamp providing visible light ($\lambda > 420$ nm) by using a 420 nm cut-off filter. After that, the resulting mixture was centrifuged and washed. The solution was evaporated under reduced pressure, and the obtained crude compound was purified by column chromatography with n-hexane/ethyl acetate (20:1) as eluent on silica gel to afford 3-arylmethyl indole derivatives.

S29. Illustration of energy level diagram for sequential FRET-associated PL and photocatalytic mechanism

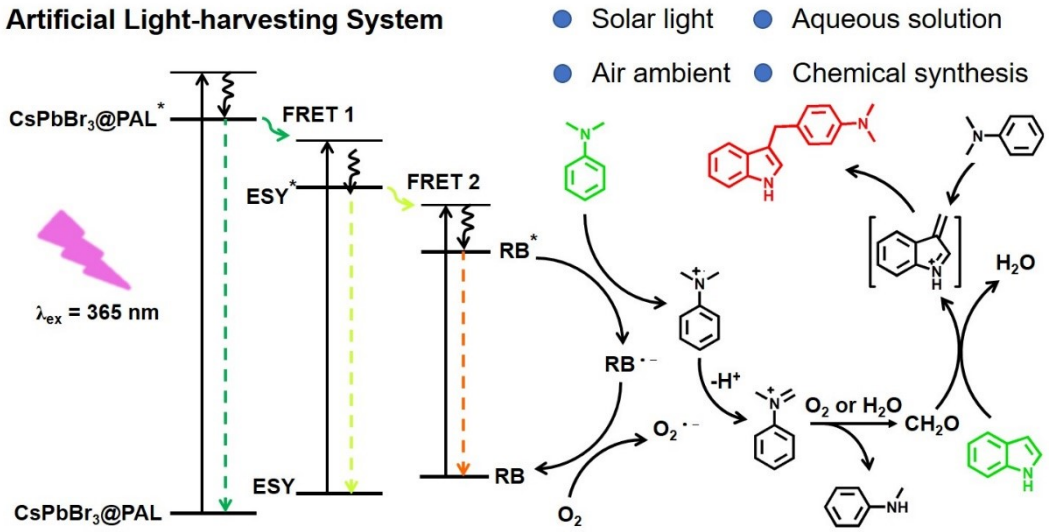

Figure S28. Illustration of energy level diagram for sequential FRET-associated PL and photocatalytic mechanism.

S30. ^{1}H NMR spectrum

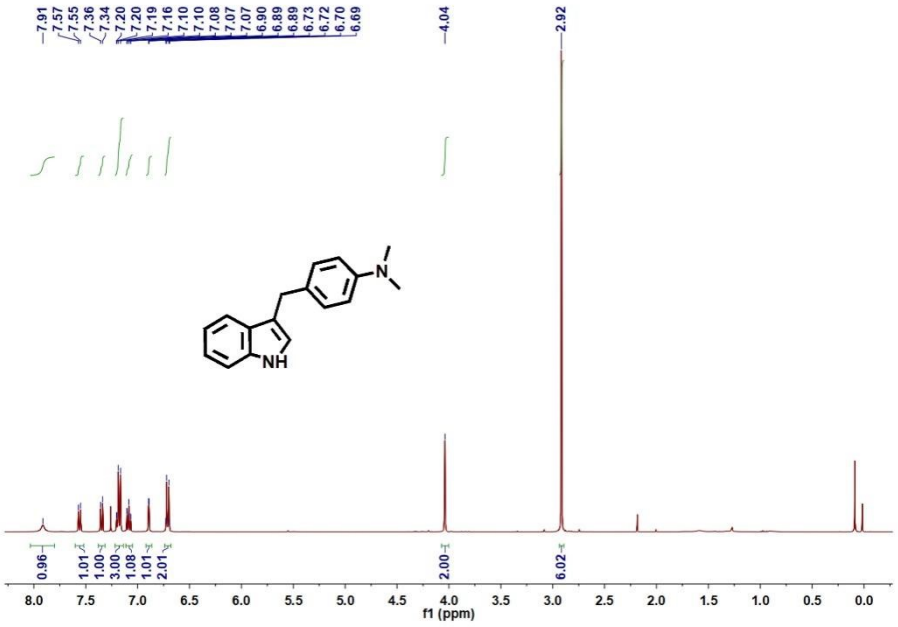

Figure S29. ^{1}H NMR spectrum (400 MHz, $CDCl_3$, 298K) of **1c**.
4-((1H-indol-3-yl)methyl)-N,N-dimethylaniline; ^{1}H NMR (400 MHz, $CDCl_3$) δ 2.92(s, 6H), 4.04(s, 2H), 6.71(m, 2H), 6.89(s, 1H), 7.07-7.10(m, 1H), 7.16-7.20(m, 3H), 7.35(d, 1H, J = 8.1 Hz), 7.56(d, 1H, J = 7.9 Hz), 7.91(s , 1H).

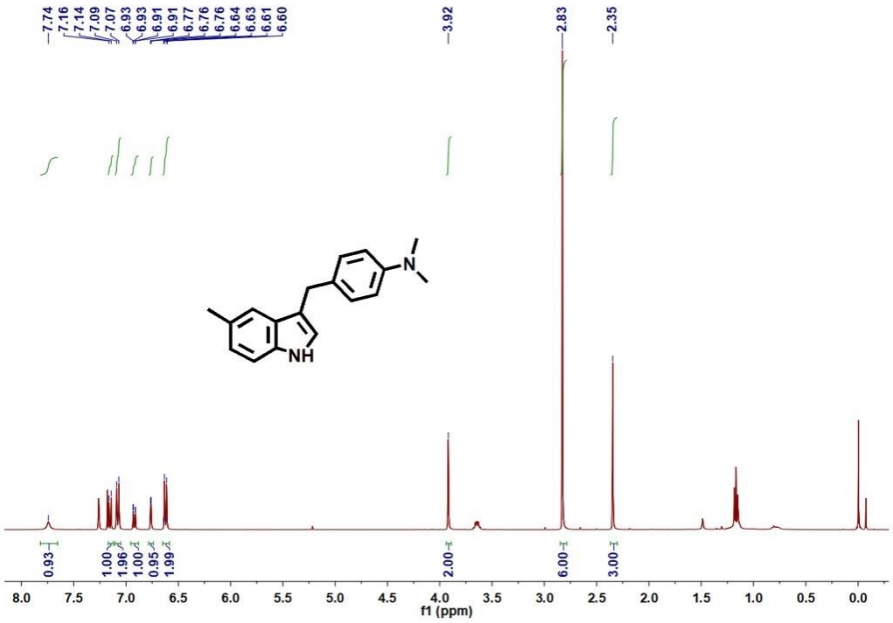

Figure S30. ^{1}H NMR spectrum (400 MHz, $CDCl_3$, 298K) of **2c**.

4-((5-methyl-1H-indol-3-yl)methyl)-N,N-dimethylaniline: ^{1}H NMR (400 MHz, $CDCl_3$) δ 2.35(s, 3H), 2.83(s, 6H), 3.92(s, 2H), 6.62(m, 2H), 6.76(s, 1H), 6.92(d, 1H, J=8.2 Hz), 7.07-7.16(m, 3H), 7.74(s, 1H).

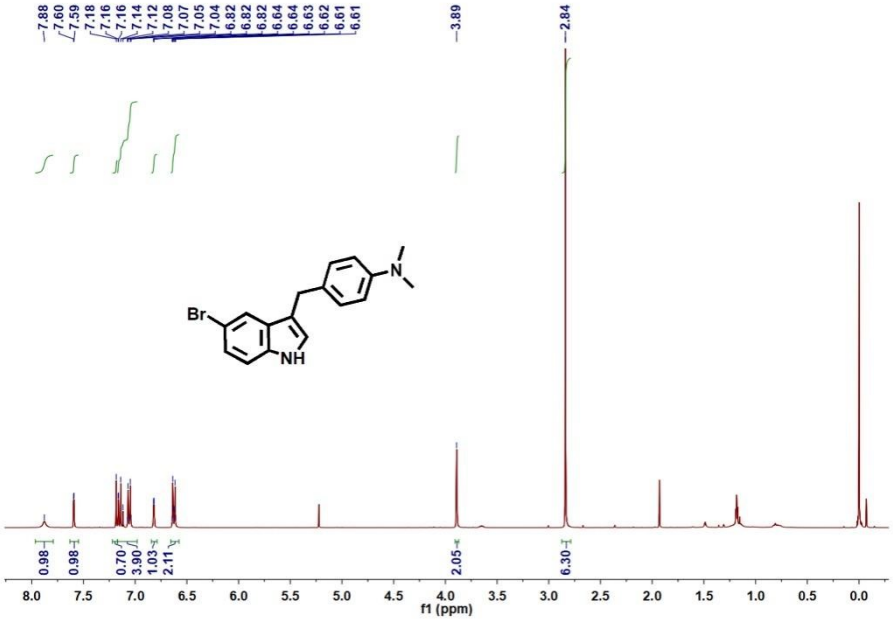

Figure S31. ^{1}H NMR spectrum (400 MHz, $CDCl_3$, 298K) of **3c**.

4-((5-bromo-1H-indol-3-yl)methyl)- N,N-dimethylaniline: ^{1}H NMR (400 MHz, $CDCl_3$) δ 2.84(s, 6H), 3.99(s, 2H), 6.63(d, 2H, J = 9.0Hz), 6.82 (s, 1H), 7.04-7.18(m, 4H), 7.59(s, 1H), 7.88(s, 1H).

S31. Additional tables

Table S2. Specific surface areas of PAL and $CsPbBr_3$@PAL calculated with BET method.

Sample	Specific Surface Area (m^2g^{-1})	Pore volume (m^3g^{-1})	pore size (nm)
PAL matrix	264.4	0.47	2.0-6.0
$CsPbBr_3$@PAL	110.1	0.38	-

Table S3. TRPL results for $CsPbBr_3$@PAL composite and $CsPbBr_3$ QDs.

Sample	τ_1(ns)	Proportion (%)	τ_2(ns)	Proportion (%)	$\tau_{av.}$(ns)
$CsPbBr_3$@PAL	19.61	71	121.64	29	48.90
$CsPbBr_3$ QDs	3.58	69	20.92	31	8.94

Table S4. Fluorescence quantum yields of $CsPbBr_3$@PAL composite (in Water).

Sample	Concentration (mg mL^{-1})	Photoluminescence quantum yields (PLQY)
$CsPbBr_3$@PAL	0.1	36.2%

Table S5. Fluorescence lifetimes of $CsPbBr_3$@PAL, ESY-$CsPbBr_3$@PAL, and RB-ESY-$CsPbBr_3$@PAL in aqueous solution.

Sample	τ_1(ns)	Proportion (%)	τ_2(ns)	Proportion (%)	$\tau_{av.}$(ns)
$CsPbBr_3$@PAL	19.61	71	121.64	29	48.90
ESY-$CsPbBr_3$@PAL[a]	2.21	87	29.00	13	5.80
ESY-$CsPbBr_3$@PAL[b]	18.04	72	121.89	28	46.74
RB-ESY-$CsPbBr_3$@PAL	4.31	84	41.94	16	10.45

Table S6. The energy transfer efficiency in aqueous solution.

Sample	Donor/acceptor ratio	Energy transfer efficiency (Φ_{ET})
ESY-$CsPbBr_3$@PAL	100:7	72.2%
RB-ESY-$CsPbBr_3$@PAL	100:7:9	65.3%

[$CsPbBr_3$@PAL] = 0.1 mg mL^{-1}, [ESY] = 1.0 mg mL^{-1}, [RB] = 1.0 mg mL^{-1}

Table S7. The RB-ESY-$CsPbBr_3$@PAL system and dyes alone catalyzed synthesis of C3-alkylated indole derivatives.

Entry	R	Yield[c] (%)	Yield[d] (%)
2	CH_3	26.6	68.2
3	Br	23.2	61.6

[c] Dyes as a photocatalyst Isolated yield

[d] RB-ESY-$CsPbBr_3$@PAL system as a photocatalyst isolated yield

S32. Supporting References

[1] Sun, S.; Yuan, D.; Xu, Y.; Wang, A.; Deng, Z., *ACS Nano* 2016, **10** (3), 3648-57.

[2] Zhang, D.; Yu, W.; Li, S.; Xia, Y.; Li, X.; Li, Y.; Yi, T., *J Am Chem Soc* 2021, **143** (3), 1313-1317.

[3] Ataka, K.-i.; Yotsuyanagi, T.; Osawa, M., *J Phys Chem C* 1996, **100** (25), 10664-10672.

[4] Posch, H. A.; Hoover, W. G.; Vesely, F. J., *Physical Review A* 1986, **33** (6), 4253-4265.

[5] Hoover, W. G.; Holian, B. L., *Physics Letters A* 1996, **211** (5), 253-257.

[6] Kohn, W.; Sham, L. J., *Physical Review* 1965, **140** (4A), A1133-A1138.

[7] Yanai, T.; Tew, D. P.; Handy, N. C., Chemical *Physics Letters* 2004, **393** (1-3), 51-57.

[8] Li, J. F.; Huang, Y. F.; Ding, Y.; Yang, Z. L.; Li, S. B.; Zhou, X. S.; Fan, F. R.; Zhang, W.; Zhou, Z. Y.; Wu, D. Y.; Ren, B.; Wang, Z. L.; Tian, Z. Q., *Nature* 2010, **464** (7287), 392-395.

[9] Schultz, Z. D.; Shaw, S. K.; Gewirth, A. A., *J. Am. Chem. Soc.* 2005, **127** (45), 15916-15922.

[10] Liu, W.-T.; Shen, Y. R., *Proc. Natl. Acad. Sci. U. S. A.* 2014, **111** (4), 1293-1297.

[11] Lefebvre C, Khartabil H, Boisson J C, et al. *ChemPhysChem*, 2018, **19** (6): 724-735.

[12] Lu, T., & Chen, F. Multiwfn: *J. Comput. Chem.*, 2012, **33** (5), 580-592.